(4)

CHEMICAL
RESEARCH,
DEVELOPMENT &
ENGINEERING
CENTER

CRDEC-TR-88076

REACTION OF MICROPARTICLES BY THE DIFFUSION OF REACTIVE GASES THROUGH POROUS SHELLS

by Glenn O. Rubel, Ph.D.
RESEARCH DIRECTORATE

James W. Gentry, Ph.D.
UNIVERSITY OF MARYLAND
College Park, MD 20742

April 1988

U.S. ARMY
ARMAMENT
MUNITIONS
CHEMICAL COMMAND

Aberdeen Proving Ground, Maryland 21010-5423

Disclaimer

The findings in this report are not to be construed as an official Department of the Army position unless so designated by other authorizing documents.

Distribution Statement

Approved for public release; distribution is unlimited.

UNCLASSIFIED
SECURITY CLASSIFICATION OF THIS PAGE

REPORT DOCUMENTATION PAGE

1a. REPORT SECURITY CLASSIFICATION UNCLASSIFIED	1b. RESTRICTIVE MARKINGS
2a. SECURITY CLASSIFICATION AUTHORITY	3. DISTRIBUTION/AVAILABILITY OF REPORT Approved for public release; distribution is unlimited.
2b. DECLASSIFICATION/DOWNGRADING SCHEDULE	
4. PERFORMING ORGANIZATION REPORT NUMBER(S) CRDEC-TR-88076	5. MONITORING ORGANIZATION REPORT NUMBER(S)
6a. NAME OF PERFORMING ORGANIZATION: CRDEC 6b. OFFICE SYMBOL (If applicable): SMCCR-RSP-B	7a. NAME OF MONITORING ORGANIZATION
6c. ADDRESS (City, State, and ZIP Code) Aberdeen Proving Ground, MD 21010-5423	7b. ADDRESS (City, State, and ZIP Code)
8a. NAME OF FUNDING/SPONSORING ORGANIZATION: CRDEC 8b. OFFICE SYMBOL (If applicable): SMCCR-RSP-B	9. PROCUREMENT INSTRUMENT IDENTIFICATION NUMBER
8c. ADDRESS (City, State, and ZIP Code) Aberdeen Proving Ground, MD 21010-5423	10. SOURCE OF FUNDING NUMBERS PROGRAM ELEMENT NO.: PROJECT NO.: 1C161102 TASK NO.: A71A WORK UNIT ACCESSION NO.:

11. TITLE (Include Security Classification)
Reaction of Microparticles by the Diffusion of Reactive Gases Through Porous Shells

12. PERSONAL AUTHOR(S)
Rubel, Glenn O., Ph.D., and Gentry, James W., Ph.D.*

13a. TYPE OF REPORT	13b. TIME COVERED	14. DATE OF REPORT (Year, Month, Day)	15. PAGE COUNT
Technical	FROM 86 Sep TO 87 May	1988 April	24

16. SUPPLEMENTARY NOTATION
*University of Maryland, College Park, MD

17. COSATI CODES			18. SUBJECT TERMS (Continue on reverse if necessary and identify by block number)
FIELD	GROUP	SUB-GROUP	Heterogeneous reaction; Surface phase; Gas phase diffusion; Crystallization; Porous shell diffusion
15	06	03	

19. ABSTRACT (Continue on reverse if necessary and identify by block number)

A new experimental technique, single particle electrodynamic balance (SPEB), was used to study the heterogeneous reaction between single acid droplets and basic gases. Experiments with phosphoric acid droplets and ammonia gas show that the droplet reaction dynamics are sequentially controlled by surface phase, gas phase diffusion-controlled, and porous shell diffusion-controlled reactions. Gas phase diffusion-controlled reactions terminate when ammonium phosphate crystallizes at the droplet surface, and porous shell diffusion-controlled reactions become rate limiting. We derive a semi-empirical model to describe the porous shell diffusion-controlled reactions of acid droplets with surface layers of crystallized solids. The model is parameterized with an effective porous shell diffusion coefficient to describe the transport of reactive gases through the porous shell. The model is compared to reaction data obtained from the SPEB
(Continued on reverse)

20. DISTRIBUTION/AVAILABILITY OF ABSTRACT ☒ UNCLASSIFIED/UNLIMITED ☐ SAME AS RPT. ☐ DTIC USERS	21. ABSTRACT SECURITY CLASSIFICATION UNCLASSIFIED
22a. NAME OF RESPONSIBLE INDIVIDUAL SANDRA J. JOHNSON	22b. TELEPHONE (Include Area Code): (301) 671-2914 22c. OFFICE SYMBOL: SMCCR-SPS-T

DD FORM 1473, 84 MAR — 83 APR edition may be used until exhausted. All other editions are obsolete.

SECURITY CLASSIFICATION OF THIS PAGE
UNCLASSIFIED

19. ABSTRACT (Continued)

for the reaction of phosphoric acid droplets layered with shells of ammonium phosphate. The characteristic pore radius of the porous shell is determined as a function of reaction condition.

PREFACE

The work described in this report was authorized under Project No. 1C161102A71A, Research in CW/CB Defense. This work was started in September 1986 and completed in May 1987.

The use of trade names or manufacturers' names in this report does not constitute an official endorsement of any commercial products. This report may not be cited for purposes of advertisement.

This report has been approved for release to the public.

Blank

CONTENTS

Blank

REACTION OF MICROPARTICLES BY THE DIFFUSION OF REACTIVE GASES THROUGH POROUS SHELLS

1. INTRODUCTION

Recently, we developed a new technique to study the heterogeneous reaction between acid aerosols and basic gases.[1] The technique, single particle electrodynamic balance (SPEB), uses both oscillating and static electric fields to stabilize single, charged droplets at a fixed point in space. The droplet mass is determined from the weight-balancing static electric field that maintains the droplet at the focal plane of a telemicroscope. By monitoring the time-dependent, weight-balancing electric field, we can analyze processes that cause changes in the droplet mass. Rubel and Gentry[1] studied the heterogeneous reaction between single phosphoric acid droplets and ammonia gas by recording the increasing weight-balancing voltage during droplet reaction. We found that the droplet reactions are sequentially controlled by surface phase, gas phase diffusion-controlled, and porous shell diffusion-controlled reactions. Observing the droplet through a telemicroscope, we noted that gas phase diffusion-controlled reactions terminate after particle crystallization.

The time of particle crystallization decreased with increasing ammonia gas partial pressure and decreasing droplet size. This correlation supported the hypothesis that the development of a critical supersaturation of ammonium phosphate initiates phosphate crystallization in the droplet. To test the hypothesis, we derived a model for the time-dependent ammonium phosphate saturation field inside the droplet.* Calculations showed that, for a wide range of experimental conditions, all droplets were characterized by the same surface supersaturation of ammonium phosphate at the time of crystallization. This result substantiated the hypothesis that a critical supersaturation of ammonium phosphate initiates the formation of a porous shell at the droplet surface. Further evidence for the formation of the surface shells was found in photographic records that

---

[1]Rubel, G.O., and Gentry, J.W., "Investigation of the Reaction Between Single Aerosol Acid Droplets and Ammonia Gas," J. Aerosol Science Vol. 15, No. 6, p 661 (1984).

*Rubel, G.O., and Gentry, J.W., Unpublished data, 1987.

showed the appearance of opaque annuli at the droplet surface at the time of crystallization.

The formation of the porous shell terminates the gas phase diffusion-controlled reactions, and porous shell diffusion-controlled reactions became rate limiting. This study was conducted to develop a semiempirical model that describes the porous shell diffusion-controlled reaction of layered micro-particles. In particular, we derive a model that predicts the porous shell diffusion-controlled reaction for phosphoric acid droplets with surface layers of ammonium phosphate. The porous shell reaction model is parameterized with an effective diffusion coefficient to describe the transport of ammonia gas through the ammonium phosphate shell. Further depletion of the phosphoric acid reactant inside the droplet is modeled after a shrinking-core reaction model. The porous shell reaction model is compared to data obtained from the SPEB. We determined the characteristic pore radius of the porous shell as a function of reaction conditions using the parallel pore model of Wheeler.[2]

2. REACTION OF ACID DROPLETS IMMERSED IN AMMONIA GAS

The use of the SPEB technique to measure the heterogeneous reaction dynamics of single acid droplets has been described in detail earlier.[1] The central component of the experimental system is the electrodynamic balance that stabilizes single, charged droplets at the null point of an ac-driven hyperboloidal electric field. The droplet weight is balanced against a static electric field that maintains the droplet at the focal plane of a telemicroscope. The heterogeneous reaction rate of the single droplet is determined from the rate at which the balancing electric field increases with time. Using a 35mm objective, the system has the additional capability to monitor the time-dependent morphology of the reacting droplet. In the earlier study, Rubel and Gentry[1] measured the heterogeneous reaction dynamics of phosphoric acid droplets immersed in ammonia gas. The investigation involved droplet sizes between 42 and 72 μm and ammonia gas partial pressures between 115 and 1000 dyn/cm^2. All experiments were conducted at one atmosphere of pressure.

Figure 1 shows the extent of reaction of phosphoric acid droplets measured as a function of time in the SPEB. The extent

---

[2]Wheeler, A., Catalysis, Vol. 2, p 105, Reinhold, New York, 1955.

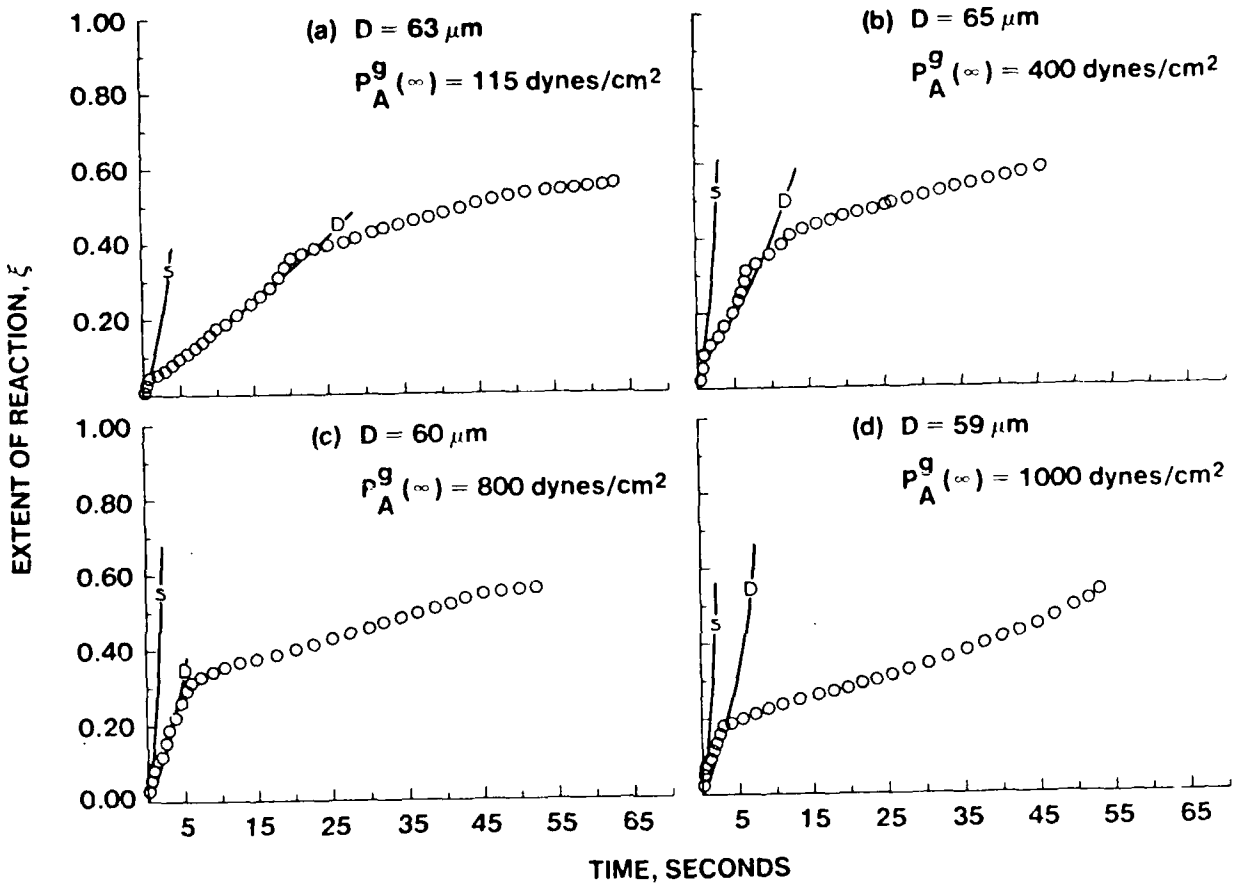

Figure 1. Comparison of Measured Extent of Reaction (0) and Theoretical Surface Phase (S) and Gas Phase Diffusion-Controlled (D) Extent of Reaction for Phosphoric Acid Droplets Immersed in Ammonia Gas.

of reaction is the ratio of the number of ammonia molecules reacted with the droplet to the number of phosphoric acid molecules initially in the droplet. This follows from the 1:1 stoichiometry of the reaction. Four separate reactions are shown, each characterized by different ammonia gas partial pressures. The data (O) is compared to theoretical surface phase (S) and gas phase diffusion-controlled (D) reaction rates.[1] Thus, the reaction dynamics are initially controlled by surface phase kinetic reactions and then by gas phase diffusion-controlled reactions. Gas phase diffusion-controlled reactions terminate after particle crystallization. The onset of particle crystallization is monitored with a telemicroscope.

3. ONSET OF PARTICLE CRYSTALLIZATION

Figure 1 shows that the time of particle crystallization decreased with increasing ammonia gas partial pressure or equivalently increasing reaction rate. For the runs shown in Figure 1, the time of particle crystallization decreased from 20 to 3.5 sec as the ammonia gas partial pressure increased from 115 to 1000 dyn/cm^2. In a later paper (unpublished data, 1987), we derived a quantitative model that predicts the ammonium phosphate saturation field inside the reacting droplet. The experimenters assumed that the reaction product, ammonium phosphate, obeyed Fick's law of diffusion and was generated at the droplet surface at a rate given by gas phase diffusion-controlled transport theory. We presented a closed form solution for the internal droplet phosphate saturation field as a function of time and ammonia gas partial pressure. Figure 2 shows the phosphate saturation fields computed at particle crystallization times of 20, 7, 4.5, and 3.5 sec, corresponding to the reactions shown i . Figure 1. At particle crystallization, the surface supersaturation of ammonium phosphate is 1.88, 1.94, 2.02, and 1.90 for the ammonia gas partial pressures of 115, 400, 800, and 1000 dyn/cm^2, respectively. Rubel and Gentry conclude that the development of a critical supersaturation of ammonium phosphate started particle crystallization.

4. THEORY

To develop a porous shell diffusion-controlled reaction model, we propose the following mechanism to describe the state of the droplet during reaction. At the time of crystallization, all droplet surfaces are characterized by the same value of the ammonium phosphate supersaturation. The excess free energy represented by the phosphate supersaturation provides the driving force for the phase transition. The phase transition relieves

the phosphate supersaturation, resulting in the formation of a porous shell at the droplet surface. In addition, an even larger annulus, of saturated ammonium phosphate is circumscribed by the porous shell. Further diffusion of ammonia gas through the shell results in the supersaturation of this phosphate-saturated annulus and the continuous build-up of the porous shell. Thus, after crystallization, the droplet reactions are controlled by the diffusion of ammonia gas through the porous shell that grows as the acid core shrinks.

To model the porous shell diffusion-controlled reaction dynamics, the salient properties of the porous shell must be specified, that is, its time-dependent thickness and the ammonia gas concentration field within the porous shell.

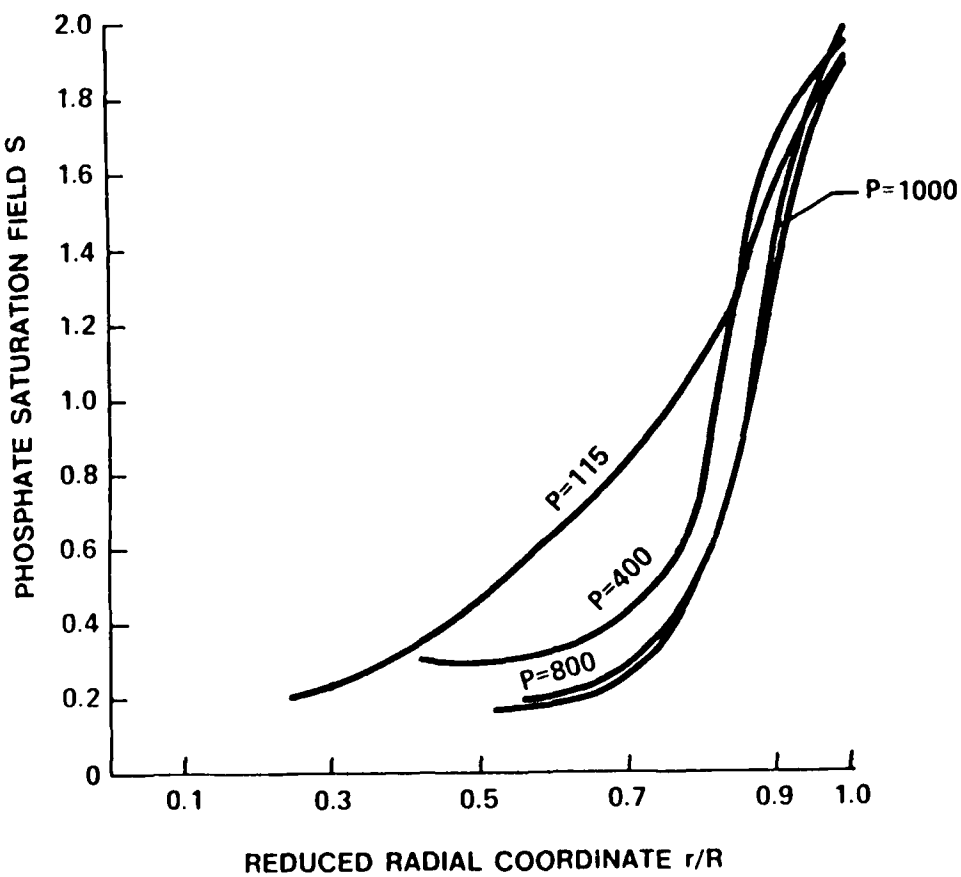

Figure 2. Theoretical Ammonium Phosphate Saturation Field Inside a Phosphoric Acid Droplet Reacting with Ammonia Gas (Ammonia gas pressure P is in units of dyn/cm^2).

4.1 Shell Thickness.

At crystallization, all ammonium phosphate exceeding the saturation concentration c_s precipitates from the solution into the body of the porous shell. As shown in Figure 2, the supersaturation zone extends inward from the droplet surface about one-tenth the droplet radius. The thickness through which the concentration field exceeds saturation is $R - \delta$, where δ is the thickness of the supersaturated zone (Figure 3a). The mass of phosphate that precipitates as a porous shell at crystallization m_{ph} is

$$m_{ph} = \int_{\delta}^{R} [c(r) - c_s] 4\pi r^2 dr \tag{1}$$

where c(r) is the radially dependent phosphate concentration at crystallization. The thickness of the shell at crystallization τ_c is defined by the relation

$$4\pi R^3/3 - 4\pi(R - \tau_c)^3/3 = m_{ph}/(1 - \epsilon)\rho_{ph} \tag{2}$$

where ρ_{ph} is the bulk density of ammonium phosphate, and ϵ is the porosity of the porous shell. In these studies, the shell thickness is much less than the droplet radius. Substituting equation 1 into equation 2, the shell thickness at crystallization can be written as

$$\tau_c = R - \left\{R^3 - 3c_s \int_{\delta}^{R} [S(r) - 1] r^2/[\rho_{ph}(1 - \epsilon)]\, dr\right\}^{1/3} \tag{3}$$

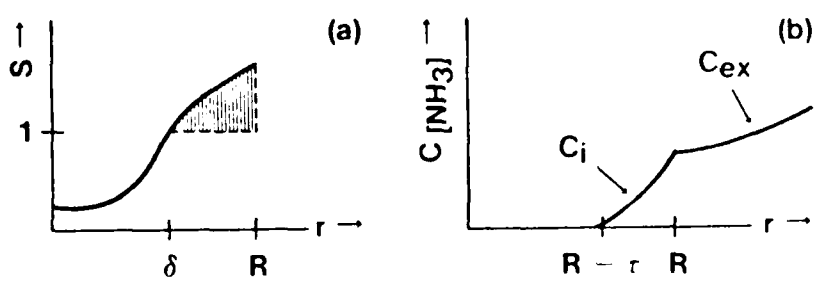

Figure 3. Schematic of Ammonium Phosphate Saturation Field before Crystallization (a) and Ammonia Gas Concentration Field Inside c_i and Outside c_{ex} the Porous Shell (b).

where $S(r)$ is the phosphate saturation ratio. The saturation ratio is defined as $S(r) \equiv c(r)/c_s$, c_s being the phosphate saturation concentration in the acid solution. As the reaction proceeds, the shell thickens. The thickness of the shell is related to the extent of droplet reaction as follows. The number of phosphate molecules n_{ph} in the droplet at time t is expressed as

$$n_{ph}(t) = n_{ph}(t_c) + 4\pi c_p^s\left\{(R - \tau_c)^3 - [R - \tau(t)]^3\right\}/3 \tag{4}$$

where $n_{ph}(t)$ is the sum of the phosphate molecules in the droplet at crystallization $n_{ph}(t_c)$ and the phosphate molecules created by the reaction between phosphoric acid molecules and ammonia gas diffusing through the porous shell. Here c_p^s is the molar volume concentration of phosphoric acid molecules in the saturated annulus. We define the extent of reaction $\&$ as $\& \equiv n_{ph}/n_p(0)$, where $n_p(0)$ is the initial number of moles of phosphoric acid in the droplet. Then, the time-dependent shell thickness is related to the extent of reaction by

$$\tau(t) = R - \left\{(R - \tau_c)^3 - 3n_p(0)[\&(t) - \&_c]/(4\pi c_p^s)\right\}^{1/3} \tag{5}$$

4.2 Ammonia Concentration Field.

The ammonia gas concentration inside the porous shell is shown qualitatively in Figure 3b. The ammonia gas concentration at the liquid acid core surface is set to zero because the reaction between the acid and ammonia molecules is rapid compared to the porous shell diffusion rate. At the droplet surface, a discontinuity exists in the slope of the concentration profile owing to the different boundary conditions imposed onto the interior c_i and exterior c_{ex} solutions for the ammonia gas concentration field. We establish the ammonia gas concentration within the porous shell by forming an imaginary sphere of radius r so that its surface lies within the porous shell. The transport rate of ammonia gas through the shell is

$$4\pi r^2 D_e \partial c_i/\partial r$$

where D_e is the effective porous shell diffusion coefficient. Under steady state conditions, the flux is independent of radius and

$$4\pi r^2 D_e \partial c_i/\partial r \equiv N = \text{constant} \tag{6}$$

Integrating equation 6 from $R - \tau$ to R and using the boundary condition $c_i(R - \tau) = 0$, the constant N is

$$N = \frac{4\pi D_e c_i(R)}{[1/(R - \tau) - 1/R]}$$

Integrating equation 6 from $R - \tau$ to r, and using the expression for N, the interior concentration field is

$$c_i(r) = \frac{c_i(R)[1/(R - \tau) - 1/r]}{[1/(R - \tau) - 1/R]} \tag{7}$$

We use mass continuity at the droplet surface, i.e.,

$$4\pi R^2 D_e \partial c_i/\partial r|_R = 4\pi R^2 D_g \partial c_{ex}/\partial r|_R \tag{8}$$

where D_g is the gas phase diffusion coefficient of ammonia to determine the surface ammonia gas concentration $c_i(R)$. With $\nabla^2 c_{ex} = 0$ and $c_{ex} = c_{ex}(\infty)$ as $r \rightarrow \infty$, the exterior solution becomes

$$c_{ex}(r) = [c_{ex}(R) - c_{ex}(\infty)]R/r + c_{ex}(\infty) \tag{9}$$

Substituting equations 7 and 9 into equation 8, the interior solution is written as

$$c_i(r) = \frac{[R/(R - \tau) - R/r]D_g c_{ex}(\infty)}{\left\{D_e + [R/(R - \tau) - 1]D_g\right\}} \tag{10}$$

4.3 Porous Shell Diffusion-Controlled Reaction Model.

The transport of ammonia gas through the porous shell is determined by substituting equation 10 into equation 8. The molar transport rate of ammonia gas is

$$dn_{NH_3}/dt = \frac{4\pi R D_e D_g c_{ex}(\infty)}{\left\{D_e + [R/(R-\tau) - 1]D_g\right\}} \tag{11}$$

Using the definition for ξ, and because the transport rate of ammonia gas is equal to the rate of production of ammonium phosphate, the porous shell diffusion-controlled reaction rate becomes

$$d\xi/dt = \frac{4\pi R D_e D_g c_{ex}(\infty)}{n_p(0)\left\{D_e + [R/(R-\tau) - 1]D_g\right\}} \tag{12}$$

Using equation 5 to express explicitly τ in terms of ξ, the porous shell diffusion controlled reaction model for a layered acid droplet with a shrinking-core is

$$(D_e-D_g)(\xi-\xi_c)-2\pi c_p^s D_g R\{[(R-\tau_c)^3-3n_p(0)(\xi-\xi_c)/(4\pi c_p^s)]^{2/3}-(R-\tau_c)^2\}/n_p(0) = 4\pi D_e D_g R c_{ex}(\infty)t/n_p(0) \tag{13}$$

where ξ_c is the extent of reaction at crystallization.

5. COMPARISON BETWEEN EXPERIMENT AND THEORY

Table 1 shows the list of conditions (i.e., droplet size, ammonia gas partial pressure P_A^g, time of crystallization t_c, and extent of reaction at crystallization) for which theory and experiment are compared. The shell thickness at crystallization as calculated from equation 3 is also shown in Table 1. For these calculations, the shell porosity ϵ is assumed to be 0.5. The shell thickness increases with increasing droplet size and decreasing ammonia gas partial pressure. For rapid

reactions, or alternatively small droplets and large ammonia gas partial pressures, thin shells form, while for large droplets and small ammonia gas pressures, thick shells form. These calculations are supported by observations with a telemicroscope that permits droplet sizing.

The best fit between theory and experiment is obtained by adjusting the value of the product $D_e(1-\epsilon)$ so that the difference between data and theory is a minimum (see Appendix). For the shrinking-core model to be valid, it is necessary that the phosphate-saturated annulus remain saturated during droplet reaction. The characteristic time for the internal liquid acid core to become uniformly mixed is given by R^2/D_l, where D_l is the liquid phase diffusion coefficient of ammonium phosphate. Using Stoke's law to estimate D_l, the characteristic time for uniform mixing of the acid core is about 300 sec. Thus, for the reaction times of interest, the saturated annulus remains saturated and the shrinking-core model is valid. As soon as this zone is depleted, the shrinking-core model is not valid. The extent of reaction at which the saturated zone is depleted is given by

$$\xi_D = \xi_c + 4\pi c_p^s \, (R - r_c)^3 - \delta^3]/n_p(0)$$

where ξ_D is the extent of reaction at which the saturated annulus is depleted. For run 46, the extent of reaction at depletion is 0.55. At this point, the porous shell/shrinking-core model is no longer valid. In the following analyses, we compare the semi-empirical model to the reaction data up to the time that the saturated zone is depleted.

Figure 4 shows the comparison between experiment and theory for the four separate runs listed in Table 1. The four reactions correspond to reactions conducted at increasing ammonia gas partial pressures. We adjust the product $D_e(1-\epsilon)$ to minimize the deviation between experiment and theory. The product decreases by an order of magnitude as the ammonia gas partial pressure increases by almost an order of magnitude. Assuming a constant porosity of 0.5, the shell diffusion coefficient decreases from 0.025 to 0.001 cm^2/sec as the ammonia gas partial pressure increases from 115 to 1000 dyn/cm^2. While it can alter the range of the diffusion coefficient variation, uncertainty in the porosity ϵ cannot account for the trend that with increasing

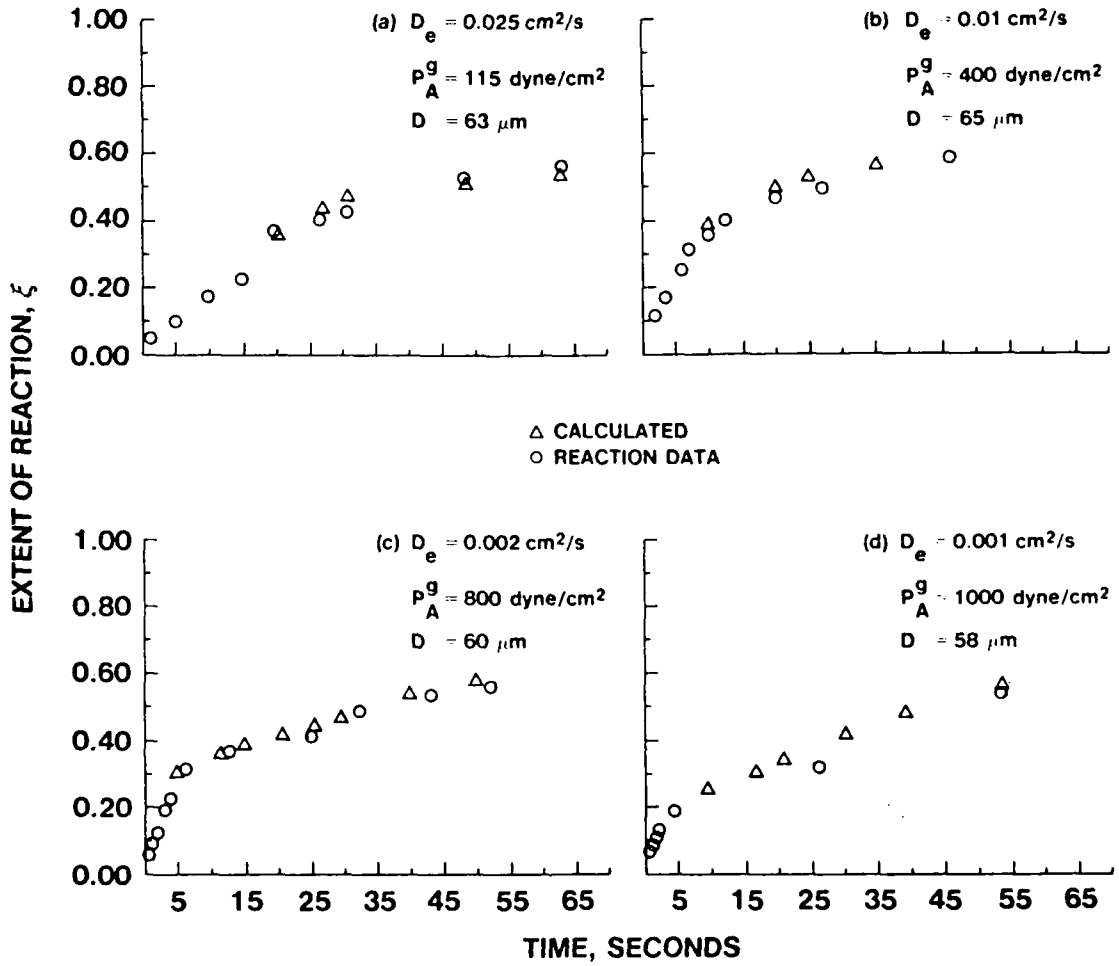

Figure 4. Comparison of Measured Extent of Reaction (0) and Theoretical Porous Shell Diffusion-Controlled Extent of Reaction (Δ) for Different Reaction Conditions. Porous Shell Diffusion-Controlled Reactions Initiated at Particle Crystallization.

ammonia gas pressure the shell diffusion coefficient decreases substantially.

Table 1. Experimental Conditions for Reactions Between Phosphoric Acid Droplets and Ammonia Gas.

Run	Radius (μm)	P_A^g(dyn/cm^2)	t_c(sec)	ξ_c	r_c(μm)
46	32	115	20.0	0.36	1.01
42	33	400	7.0	0.31	0.99
50	30	800	4.5	0.30	0.69
48	29	1000	3.5	0.18	0.62

According to Wheeler's parallel pore model,[2] the porous shell diffusion coefficient is related to the single pore diffusion coefficient D_p by the relation

$$D_e = \frac{\epsilon}{\kappa^2} D_p \tag{14}$$

where ϵ is the porosity of the shell defined as the ratio of the pore surface area to the shell surface area. The tortuosity κ describes the deviation of the pore from an ideal cylinder. The diffusion coefficient decreases if, the individual pore diffusion coefficient decreases, the porosity of the shell decreases or the tortuosity increases. In this study, we assume that the pore tortuosity is equal to unity. The Appendix shows that the porous shell diffusion coefficient is inversely proportional to $(1-\epsilon)$. This fact arises from the reciprocal dependence between the shell thickness and the shell diffusion coefficient. Explicitly showing the dependence on ϵ, equation 14 becomes

$$D_p = \frac{A}{\epsilon(1 - \epsilon)} \tag{15}$$

where A is the value of the product $D_e(1-\epsilon)$ that satisfies equation 13. Recall that for each run, A will assume a different value. Since the product $\epsilon(1 - \epsilon)$ does not vary significantly

(less than a factor of two) as the porosity varies from 0.2 to 0.8, we use a mean value approach. For $\epsilon = 0.5$, the pore diffusion coefficient is $D_p = 4A$.

This relation permits the evaluation of the individual pore diffusion coefficient from knowledge of the parameter A, the evaluation of which does not require an explicit knowledge of the shell porosity.

If the capillary radius is much less than the mean free path of the gas, then diffusion through the capillary is described by Knudsen flow. The individual pore diffusion coefficient for a cylindrical capillary is

$$D_p = 4r_c(2KLT/\pi M)^{1/2}/3 \tag{16}$$

where r_c is the individual pore radius, K is Boltzmann constant, L is Avagadro's number, T is the temperature, and M is the molecular weight of the diffusing gas. As the capillary radius decreases, the diffusion coefficient decreases. Table 2 shows the pore radius calculated by substituting the experimentally determined pore diffusion coefficient (equation 15) into the Knudsen flow diffusion coefficient (equation 16). As the ammonia gas partial pressure increases, the pore radius decreases. The dependence of the pore radius on the ammonia gas partial pressure, or equivalently the reaction rate, explains the phenomenon of encapsulation that is observed at ammonia gas partial pressures exceeding 1000 dyn/cm^2. At these pressures, the pore size could be so small that the ammonia gas molecule is too large to penetrate the individual pore. That is, the shell acts like a molecular sieve. Indeed, the spherical equivalent radius of an ammonia gas molecule is 1.54 Angstroms, and Table 2 shows evidence that the pore radius is approaching the physical radius of the ammonia gas molecule.

6. SUMMARY

We derive a semiempirical reaction model that describes the porous shell diffusion-controlled reaction of layered droplets. Specifically, we present a model for the reaction of phosphate-layered acid droplets immersed in ammonia gas. The model is parameterized with an effective shell diffusion coefficient to describe the transport of ammonia gas through the phosphate shell. The further depletion of phosphoric

acid reactant inside the droplet is modeled after a shrinking-core model. We compared the reaction model to data obtained from the electrodynamic balance. We found that the shell diffusion coefficient depends on the droplet reaction rate, decreasing more than an order of magnitude as the ammonia gas pressure increases by an order of magnitude. Furthermore, the average pore radius of the shell decreases with increasing droplet reaction rate. This accounts for the observed negative correlation between the shell diffusion coefficient and ammonia gas pressure. For large ammonia gas partial pressures, the shell diffusion coefficient decreases to zero, and the droplet is encapsulated. Future work will be directed toward the determination of the porosity of the phosphate shells, and thereby a more accurate determination of the shell diffusion coefficient.

Table 2. Pore Radius as a Function of Ammonia Gas Partial Pressure.

r_c(Å)	$P_A{}^g$(dyn/cm^2)
246.24	115
98.56	400
9.84	1000

APPENDIX

THE DEPENDENCE OF THE SHELL DIFFUSION COEFFICIENT ON THE POROSITY

Blank

APPENDIX

THE DEPENDENCE OF THE SHELL DIFFUSION COEFFICIENT ON THE POROSITY

The dependence of the shell diffusion coefficient D_e on the porosity ϵ of the shell is derived from the following considerations. Using the definition

$$A = 3c_s \int_{\delta}^{R} [S(r) - 1] r^2 dr / \rho_{ph}$$

we can rewrite equation 3 as

$$\tau_c = R - [R^3 - A/(1 - \epsilon)]^{1/3}$$

Since $\tau_c << R$, $A/[R^3(1 - \epsilon)] << 1$, and the shell thickness reduces to

$$\tau_c = R - R\left\{1 - A/[3 R^3(1 - \epsilon)]\right\}$$

$$= \frac{A}{3R^2(1 - \epsilon)} \qquad \text{(A)}$$

Thus, as the shell porosity increases, the shell thickness at crystallization increases. To determine the dependence of the shell diffusion coefficient on the shell porosity, equation A is substituted into equation 13. Preliminary to this substitution, we use the approximation

$$(R - \tau_c)^3 >> 3n_p(0)(\mathcal{E} - \mathcal{E}_c)/(4\pi c_p^s) \qquad \text{(B)}$$

to simplify equation 13. Approximation equation B is clearly valid during the early stages of reaction when $\mathcal{E} = \mathcal{E}_c$. Using this approximation to expand the expression in equation 13, we obtain

$$(D_e - D_g)\ (\mathcal{E}-\mathcal{E}_c) + (\mathcal{E}-\mathcal{E}_c)D_gR/(R - r_c) = 4\pi D_eD_gRc_{ex}(\infty)+/n_p(O) \qquad (C)$$

With r_c<<R, equation C becomes

$$\left(1 + \frac{D_g\, r_c}{D_eR}\right)\left(\mathcal{E} - \mathcal{E}_c\right) = 4\pi D_gRc_{ex}(\infty)t/n_p(0) \qquad (D)$$

Thus, holding all pertinent parameters constant, the ratio r_c/D_e must remain constant. Using equation A, the dependence of the shell diffusion coefficient on the porosity is

$$D_e = \text{constant}/(1 - \epsilon)$$